# Supporting Information

## $Fe_3O_4$ Quantum Dots Decorated $MoS_2$ Nanosheet Arrays on Graphite Paper as Free-Standing Sodium-Ion Batteries anode

Dezhi Kong,[a b] Chuanwei Cheng,* [a] Ye Wang,*[b] Zhixiang Huang,[b] Bo Liu,[b] Yew Von Lim,[b] Qi Ge,[b] and Hui Ying Yang * [b]

[a] *Shanghai Key Laboratory of Special Artificial Microstructure Materials and Technology, School of Physics Science and Engineering, Tongji University, Shanghai 200092, P. R. China. E-mail: cwcheng@tongji.edu.cn*

[b] *Pillar of Engineering Product Development, Singapore University of Technology and Design, 8 Somapah Road, Singapore 487372, Singapore. E-mail: yanghuiying @sutd.edu.sg*

* Corresponding authors: [a] cwcheng@tongji.edu.cn; [b]yewang@sutd.edu.sg [c] yanghuiying@sutd.edu.sg

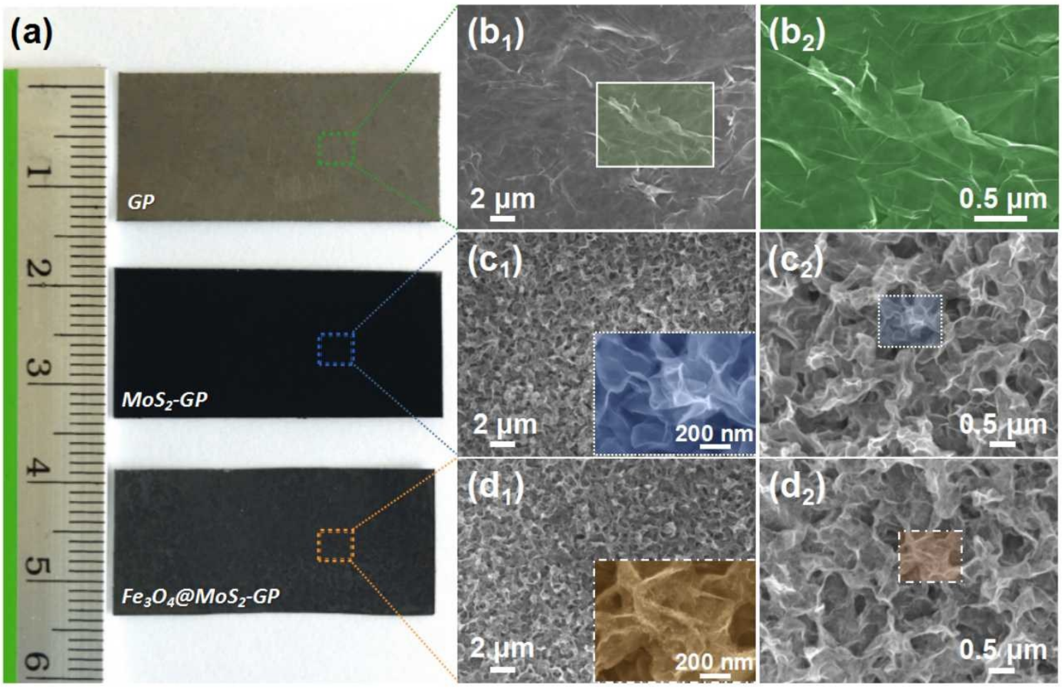


**Figure S1** (a) Photographs of graphite paper substrate, $MoS_2$ NSAs on graphite paper and $Fe_3O_4$@$MoS_2$ NSAs composite on graphite paper; ($b_1$, $b_2$) Low- and high-magnification SEM images of graphite paper substrate; ($c_1$, $c_2$) Low- and high-magnification SEM images of $MoS_2$ NSAs; ($d_1$, $d_2$) Low- and high-magnification SEM images of $Fe_3O_4$@$MoS_2$ NSAs composite.

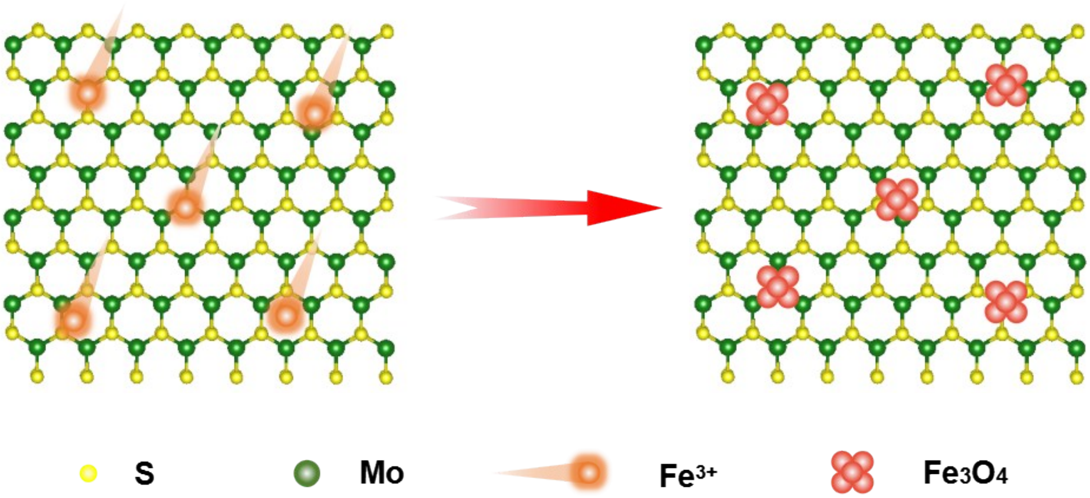


**Figure S2** Formation mechanism of $Fe_3O_4$@$MoS_2$ nanostructure.

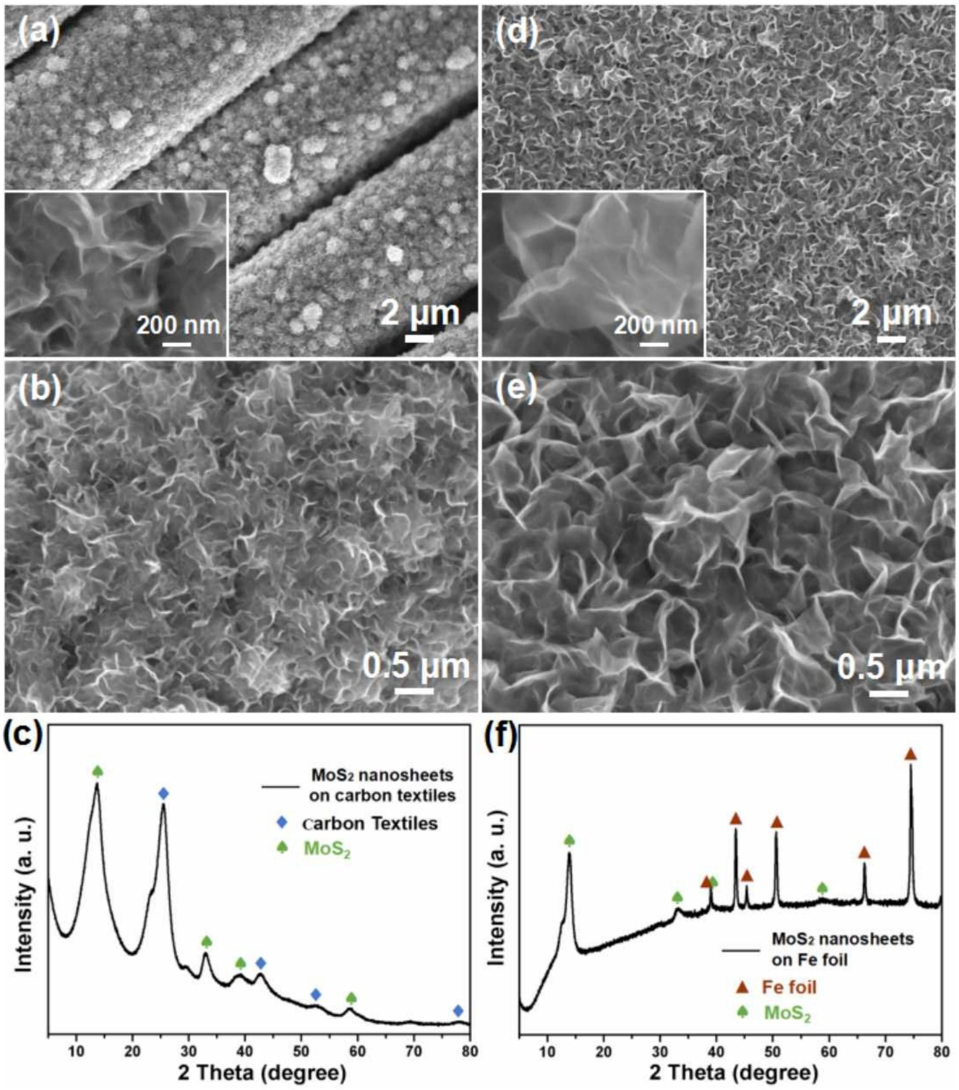


**Figure S3** (a, b) SEM images of the $MoS_2$ nanosheet arrays on carbon textiles substrate; (c) XRD pattern of the $MoS_2$ nanosheet arrays on carbon textiles substrate, confirming the composition; (d, e) SEM images of $MoS_2$ nanosheet arrays on Fe foil substrate; (f) XRD pattern of the $MoS_2$ nanosheet arrays on Fe foil substrate, confirming the composition. All these samples were fabricated based on the protocol proposed in Fig. 1, clearly demonstrating its generality.

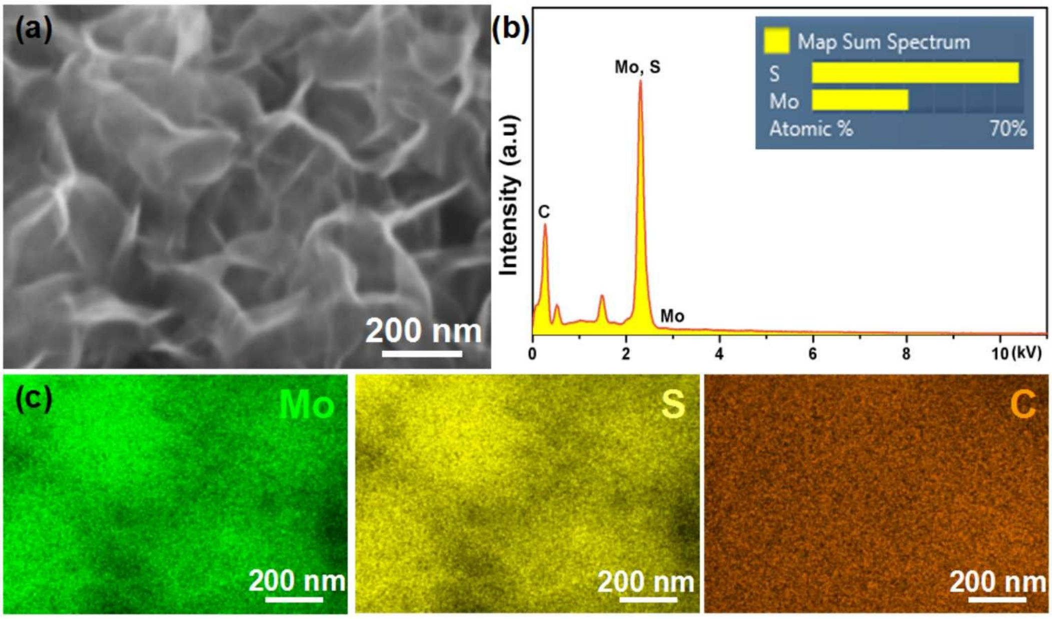


**Figure S4** (a) SEM images the $MoS_2$ nanosheets; (b) EDS microanalysis and the corresponding elemental contents on selected areas of the $MoS_2$ nanosheets; (c) EDS elemental mappings of Mo, S and C for the $MoS_2$ nanosheets with corresponding SEM image.

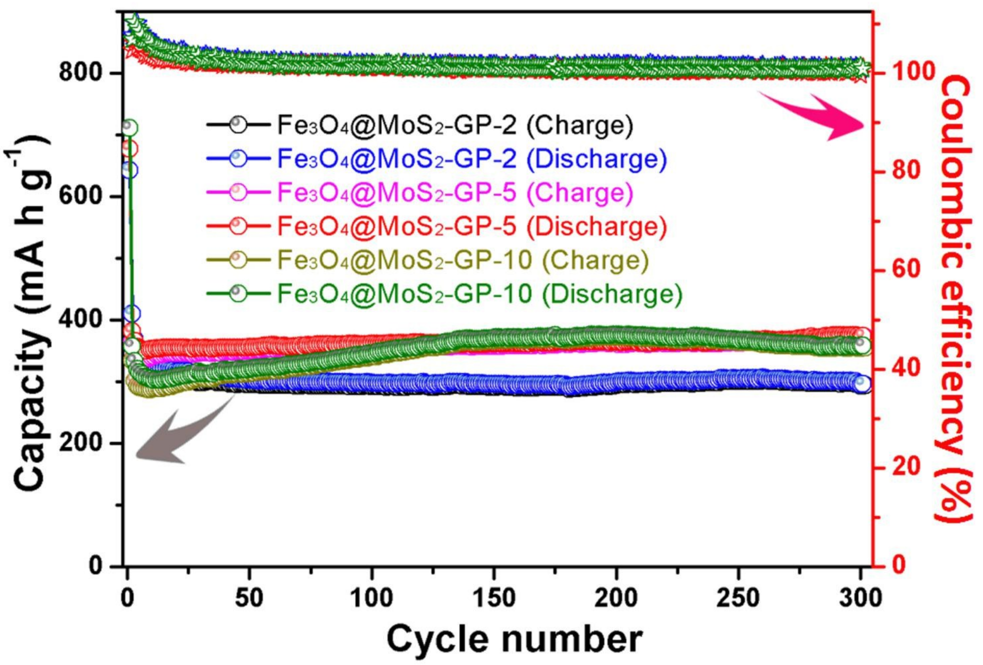


**Figure S5** Cycling performance of the $Fe_3O_4$@$MoS_2$-GP composites during the second hydrothermal process at various reaction stages by setting the reaction time to 2 h, 5 h, and 10 h (marked as $Fe_3O_4$@$MoS_2$-GP-2, $Fe_3O_4$@$MoS_2$-GP-5, and $Fe_3O_4$@$MoS_2$-GP-10, respectively) at a constant current density of 400 mA $g^{-1}$.

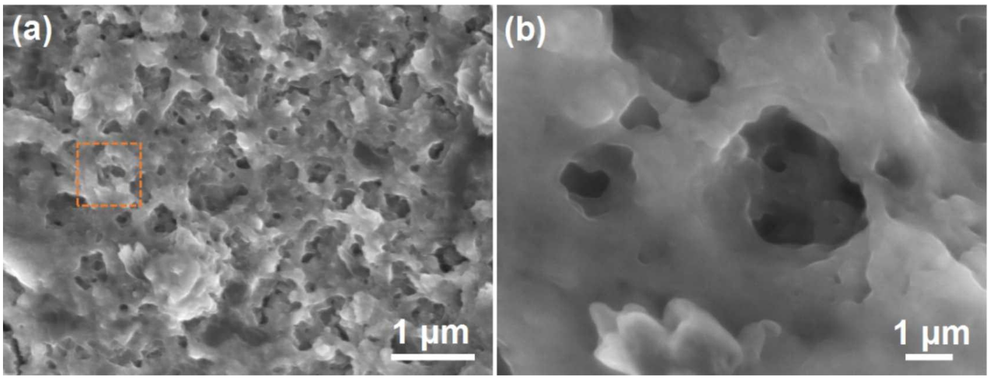


**Figure S6** SEM images of $Fe_3O_4$@$MoS_2$-GP-10 anodes after 300 times cycling.

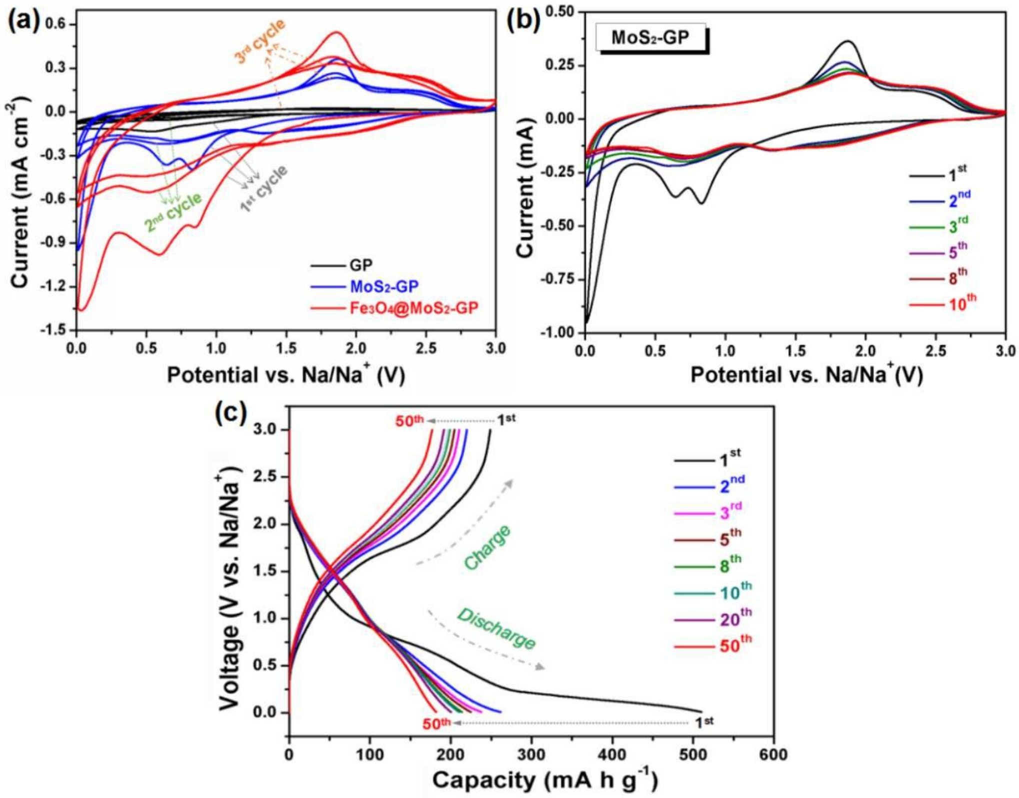


**Figure S7** (a) The initial three CV curves for GP, $MoS_2$-GP, $Fe_3O_4$@$MoS_2$-GP, recorded at a scan of 0.1 mV $s^{-1}$; (e) Representative CV curves of an electrode based on the $MoS_2$-GP obtained at a voltage range of 0 to 3.0 V (vs $Na/Na^+$) and potential scan rate of 0.1 mV $s^{-1}$; (b) Voltage profiles plotted for the first, second, third, $5^{th}$, $8^{th}$, $10^{th}$, $20^{th}$ and $50^{th}$ cycles of the $MoS_2$-GP electrode at a current density of 100 mA $g^{-1}$.

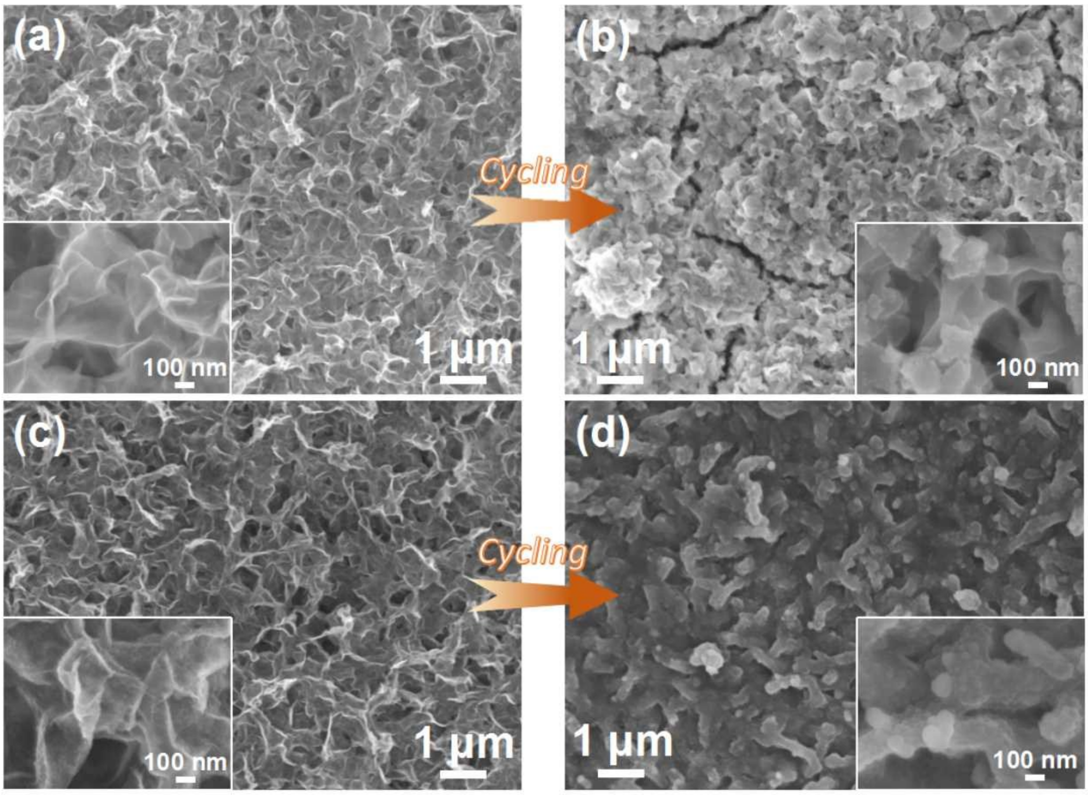


**Figure S8** SEM images of (a) $MoS_2$, (c) $Fe_3O_4$@$MoS_2$ anodes before cycling, and (b) $MoS_2$, (d) $Fe_3O_4$@$MoS_2$ anodes after 300 times cycling.

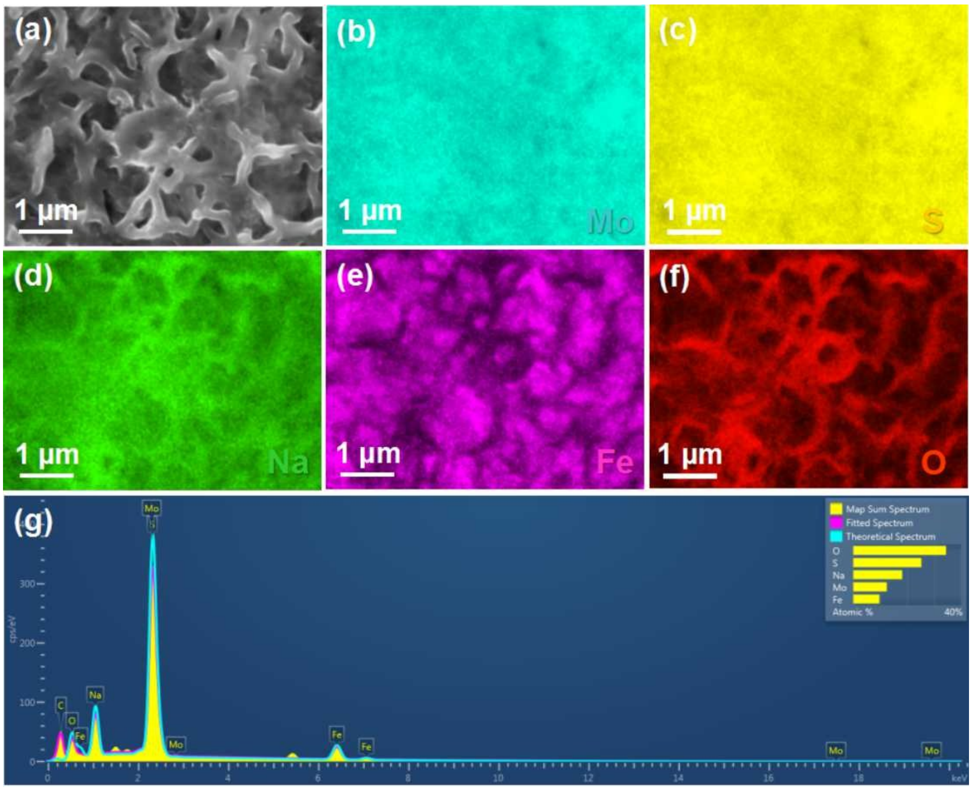


**Figure S9** (a) SEM image of a cracked $Fe_3O_4$@$MoS_2$ anodes after 300 times cycling; The corresponding EDS elemental dot-mapping images of (b) Mo, (c) S, (d) Na, (e) Fe and (f) O elements; (g) EDS microanalysis and the corresponding elemental contents on selected areas of the $Fe_3O_4$@$MoS_2$ anodes after 300 cycles.

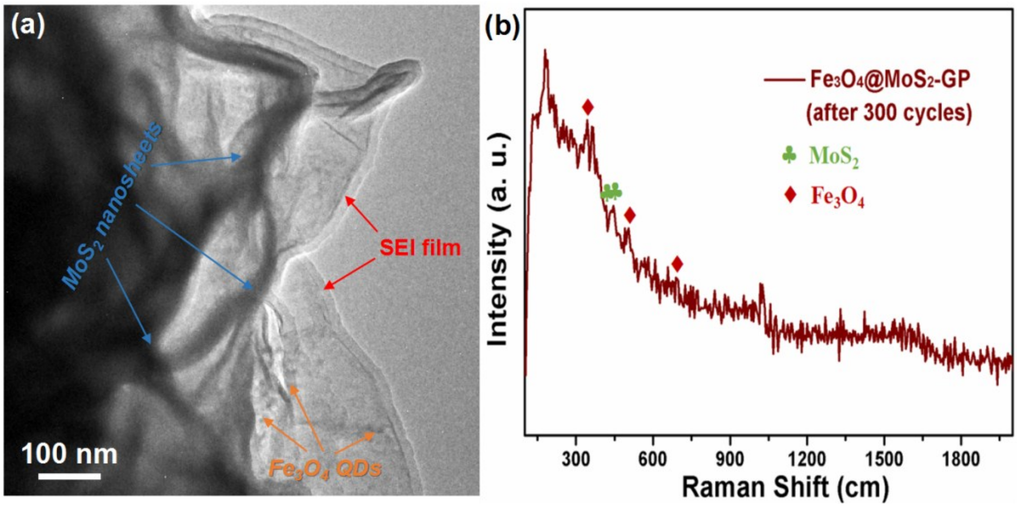


**Figure S10** TEM image (a) and Raman spectra (b) of $Fe_3O_4$@$MoS_2$ composite after 300 times cycling.

**Table S1** The comparison of electrochemical performance for $MoS_2$ nanostructures and $MoS_2$-based composite nanomaterials prepared by different methods.

| Electrode description | Specific capacity (vs. Na/Na⁺) | High rate capability (vs. Na/Na⁺) | Cycling stability (%) | Ref. |
|---|---|---|---|---|
| $Fe_3O_4$@$MoS_2$-GP composite | 468 mAh $g^{-1}$ at 100 mA $g^{-1}$ | 231 mA h $g^{-1}$ at 3200 mA $g^{-1}$ | ~72.5% after 300 cycles at 100 mA $g^{-1}$ | This work |
| $MoS_2$@C-CMC | 446 mAh $g^{-1}$ at 20 mA $g^{-1}$ | 205 mAh $g^{-1}$ at 1000 mA $g^{-1}$ | ~79.4% after 100 cycles at 80 mA $g^{-1}$ | [1] |
| Asprepared $MoS_2$ nanosheet arrays | 530 mAh $g^{-1}$ at 40 mA $g^{-1}$ | 251 mAh $g^{-1}$ at 320 mA $g^{-1}$ | ~72.8% after 100 cycles at 40 mA $g^{-1}$ | [2] |
| $MoS_2$/Graphene composite | ~550 mAh $g^{-1}$ at 20 mA $g^{-1}$ | 352 mAh $g^{-1}$ at 640 mA $g^{-1}$ | ~50.8% after 100 cycles at 67 mA $g^{-1}$ | [3] |
| $MoS_2$ microflowers | 595 mAh $g^{-1}$ at 67 mA $g^{-1}$ | 240 mAh $g^{-1}$ at 6700 mA $g^{-1}$ | ~50.8% after 50 cycles at 80 mA $g^{-1}$ | [4] |
| $MoS_2$/Graphene composite paper | 240 mAh $g^{-1}$ at 25 mA $g^{-1}$ | 173 mAh $g^{-1}$ at 200 mA $g^{-1}$ | ~83% after 20 cycles at 25 mA $g^{-1}$ | [5] |
| $MoS_2$-$PEO_{2L}$ nanocomposite | 185 mAh $g^{-1}$ at 50 mA $g^{-1}$ | 112 mA h $g^{-1}$ at 1000 mA $g^{-1}$ | ~65.8% after 70 cycles at 50 mA $g^{-1}$ | [6] |
| Yolk-shell SnS-$MoS_2$ composite microspheres | 453 mAh $g^{-1}$ at 200 mA $g^{-1}$ | 238 mA h $g^{-1}$ at 7000 mA $g^{-1}$ | 89% after 100 cycles at 500 mA $g^{-1}$ | [7] |
| $MoS_2$/SWNT composite | 437 mAh $g^{-1}$ at 50 mA $g^{-1}$ | 192 mA h $g^{-1}$ at 20000 mA $g^{-1}$ | ~95% after 100 cycles at 200 mA $g^{-1}$ | [8] |
| $HfO_2$-coated $MoS_2$ nanosheet | 613 mA h $g^{-1}$ at 100 mA $g^{-1}$ | 347 mA h $g^{-1}$ at 1000 mA $g^{-1}$ | 91% after 50 cycles at 100 mA $g^{-1}$ | [9] |
| $TiO_2$-coated $MoS_2$ nanofiber | ~740 mA h $g^{-1}$ at 100 mA $g^{-1}$ | 510 mA h g-1 at 2500 mA $g^{-1}$ | 64% after 30 cycles at 100 mA $g^{-1}$ | [10] |
| $TiO_2$-B/$MoS_2$ nanowire array | 214 mA h $g^{-1}$ at 20 mA $g^{-1}$ | 48 mA h $g^{-1}$ at 4000 mA $g^{-1}$ | ~89.2% after 100 cycles at 20 mA $g^{-1}$ | [11] |
| $MoS_2$ /C nanospheres | 520 mA h $g^{-1}$ at 67 mA $g^{-1}$ | 390 mA h $g^{-1}$ at 1340 mA $g^{-1}$ | ~77.5% after 50 cycles at 67 mA $g^{-1}$ | [12] |
| Mesoporous $MoS_2$/C-31 microspheres | 481 mA h $g^{-1}$ at 100 mA $g^{-1}$ | 244 mA h $g^{-1}$ at 20000 mA $g^{-1}$ | ~94% after 100 cycles at 100 mA $g^{-1}$ | [13] |
| $MoS_2$-CNFs film | 381.7 mA h $g^{-1}$ at 100 mA $g^{-1}$ | 186.3 mA h $g^{-1}$ at 2000 mA $g^{-1}$ | 74.8% after 600 cycles at 100 mA $g^{-1}$ | [14] |
| $MoS_2$/rGO composite | 575 mA h $g^{-1}$ at 100 mA $g^{-1}$ | 406 mA h $g^{-1}$ at 1000 mA $g^{-1}$ | 94% after 50 cycles at 100 mA $g^{-1}$ | [15] |
| $MoS_2$/Graphene Composites | 491.7 mA h $g^{-1}$ at 50 mA $g^{-1}$ | 247.2 mA h $g^{-1}$ at 2000 mA $g^{-1}$ | 81% after 200 cycles at 100 mA $g^{-1}$ | [16] |
| Multiwalled carbon@$MoS_2$@carbon nanocables | ~968 mA h $g^{-1}$ at 70 mA $g^{-1}$ | 817 mA h $g^{-1}$ at 7000 mA $g^{-1}$ | 77% after 200 cycles at 700 mA $g^{-1}$ | [17] |
| $MoS_2$@C nanotubes | 610 mA h $g^{-1}$ at 50 mA $g^{-1}$ | 370 mA h $g^{-1}$ at 2500 mA $g^{-1}$ | 80% after 200 cycles at 500 mA $g^{-1}$ | [18] |
| $MoS_2$@ACNTs | 572 mA h $g^{-1}$ at 100 mA $g^{-1}$ | 396 mA h $g^{-1}$ at 1600 mA $g^{-1}$ | ~72% after 150 cycles at 500 mA $g^{-1}$ | [19] |
| 3D $MoS_2$ nanosheet/CNTs composite | 540 mA h $g^{-1}$ at 50 mA $g^{-1}$ | 328.4 mA h $g^{-1}$ at 500 mA $g^{-1}$ | 89.3% after 100 cycles at 50 mA $g^{-1}$ | [20] |

## References

[1] X. Q. Xie, T. Makaryan, M. Q. Zhao, K. L. V. Aken, Y. Gogotsi and G. X. Wang, *Adv. Energy Mater.*, 2016, 6, 1502161.

[2] D. W. Su, S. X. Dou and G. X. Wang, *Adv. Energy Mater.*, 2015, 5, 1401205.

[3] P. R. Kumar, Y. H. Jung and D. K. Kim, *RSC Adv.*, 2015, 5, 79845-79851.

[4] X. Q. Xie, Z. M. Ao, D. W. Su, J. Q. Zhang and G. X. Wang, *Adv. Funct. Mater.*, 2015, 25, 1393-1403.

[5] L. David, R. Bhandavat and G. Singh, ACS Nano, 2014, 8, 1759-1770.

[6] Y. F. Li, Y. L. Liang, F. C. R. Hernandez, H. D. Yoo, Q. Y. An and Y. Yao, *Nano Energy*, 2015, 15, 453-461.

[7] S. H. Choi and Y. C. Kang, *ACS Appl. Mater. Interfaces*, 2015, 7, 24694-24702

[8] Y. P. Liu, X. Y. He, D. Hanlon, A. Harvey, J. N. Coleman and Y. G. Li, *ACS Nano*, 2016, 10, 8821-8828.

[9] B. Ahmed, D. H. Anjum, M. N. Hedhili and H. N. Alshareef, *Small*, 2015, 11, 4341-4350.

[10] W. H. Ryu, J. W. Jung, K. Park, S. J. Kim and I. D. Kim, *Nanoscale*, 2014, 6, 10975-10981.

[11] J. Y. Liao, B. D. Luna and A. Manthiram, *J. Mater. Chem. A*, 2016, 4, 801-806.

[12] J. J. Wang, C. Luo, T. Gao, A. Langrock, A. C. Mignerey and C. S. Wang, *Small*, 2015, 11, 473-481.

[13] Y. Y. Lu, Q. Zhao, N. Zhang, K. X. Lei, F. J. Li and J. Chen, *Adv. Funct. Mater.*, 2016, 26, 911-918.

[14] X. Q. Xiong, W. Luo, X. L. Hu, C. J. Chen, L. Qie, D. F. Hou and Y. H. Huang, *Sci. Rep.*, 2015, 5, 09254.

[15] T. S. Sahu and S. Mitra, *Sci. Rep.*, 2015, 5, 12571.

[16] Y. X. Wang, S. L. Chou, D. Wexler, H. K. Liu and S. X. Dou, *Chem. Eur. J.*, 2014, 20, 9607-9612.

[17] Y. Wang, Q. T. Qu, G. C. Li, T. Gao, F. Qian, J. Shao, W. J. Liu, Q. Shi and H. H. Zheng, *Small*, 2016, 12, 6033-6041.

[18] X. Q. Zhang, X. N. Li, J. W. Liang, Y. C. Zhu and Y. T. Qian, *Small*, 2016, 12, 2484-2491.

[19] X. Xu, D. M. Yu, H. Zhou, L. S. Zhang, C. H. Xiao, C. W. Guo, S. W. Guo and S. J. Ding, *J. Mater. Chem. A*, 2016, 4, 4375-4379.

[20] S. Zhang, X. B. Yu, H. L. Yu, Y. J. Chen, P. Gao, C. Y. Li and C. L. Zhu, *ACS Appl. Mater. Interfaces*, 2014, 6, 21880-21885.